Materials Advances

ROYAL SOCIETY OF CHEMISTRY

PAPER

View Article Online
View Journal | View Issue

Check for updates

Cite this: *Mater. Adv.*, 2022, 3, 7918

The effect of multiple ion substitutions on halide ion migration in perovskite solar cells†

Samuel R. Pering *‡ and Petra J. Cameron

Lead halide perovskites are mixed electronic-ionic conductors. Ionic mobility is related to device stability; the more favourable ion migration is, the sooner material degradation occurs. The highest efficiency perovskite materials, such as $Cs_{0.05}(FA_{0.83}MA_{0.17})_{0.95}Pb(I_{0.83}Br_{0.17})_3$,include multiple substitutions into the parent $FAPbI_3$ structure. Despite the high efficiencies that multi cation and anion cells can achieve, there is still a poor understanding of the effect of mutiple substitutions on ion mobility within the perovskite itself. In this report we use electrochemical impedance spectroscopy to evaluate the effect of ion substitution at multiple sites on the activation energy for iodide diffusion. The results demonstrate that crystal lattice subsitutions have a significant effect on the activation energy. The addition of smaller cations into the FAPI lattice greatly reduces the barrier to iodide diffusion. When substitutions at multiple lattice sites are made, as in the triple cation perovskite, $Cs_{0.05}(FA_{0.83}MA_{0.17})_{0.95}Pb(I_{0.83}Br_{0.17})_3$, the activation energy of iodide diffusion is 0.81 eV. This is considerably higher than the experimental values obtained for methylammonium lead iodide and furthers understanding of the effect of multiple substitutions on perovskite stability.

Received 1st June 2022,
Accepted 19th August 2022

DOI: 10.1039/d2ma00619g

rsc.li/materials-advances

Open Access Article. Published on 23 August 2022. Downloaded on 5/3/2026 9:02:49 AM.
This article is licensed under a Creative Commons Attribution 3.0 Unported Licence.

Introduction

Since their introduction perovskite solar cells have risen rapidly to commercially competitive efficiencies.[1,2] Wide-ranging research into this technology has been enabled by abundant source materials and simple fabrication methods.[3] Recently, research has focussed on improving the long term stability of Perovskite Solar Cells (PSCs),[4,5] and developing manufacturing processes that can be used in upscaled production.[6,7] The stability of lead halide perovskites has long been a thorn in the side of their development, as the most widely studied perovskite, methylammonium lead iodide (MAPI), is unstable with regards to heat, light and water.[8–11] Solar cell stability is linked to the diffusion of ions within the perovskite lattice, which cause the hysteresis phenomenon in the short term, and in the long term can lead to degradation of the cell.[12–14] One way of observing this ion movement in perovskites is by Electrochemical Impedance Spectroscopy (EIS). An example spectrum for a methylammonium lead iodide based cell is given in Fig. 1. The plot highlights the high (HF), mid (MF) and low (LF) frequency responses that we typically see for MAPI cells in our lab, the origin of these three different responses will be discussed in the next section. The low frequency impedance response of PSC is strongly affected by ion migration. In this paper impedance is measured around open circuit under illumination. At low modulation frequencies the ions are able to move in response to the applied voltage and this field dependent ionic distribution modifies the measured current. If the time constant for the low frequency response is plotted as a function of temperature, activation energies of 0.4–0.6 eV are obtained. These values are similar to computational and experimental values of iodide diffusion.[15–17] Cation migration has also been observed in perovskite solar cells, usually with higher activation energies to iodide migration.[18] In our previous work we have looked at cells made from MAPI, or MAPI that includes of low amounts of A-site substitution.[19–24] Although the most well explored by EIS, MAPI does not make the most efficient, or the most stable PSC. High efficiency PSC use $Cs_{0.05}(FA_{0.83}MA_{0.17})_{0.95}Pb(I_{0.83}Br_{0.17})_3$, which produces cells with >23% efficiency.[2] The parent structure in this case is FAPI, which is cubic in its black phase. MAPI is usually tetragonal as formed.[25,26] Formamidinium lead iodide, (FAPI) has a smaller band gap than MAPI, closer to the ideal for solar cells.[1,27,28] The cubic structure of FAPI is however very unstable, and degrades readily to a non-perovskite δ-phase.[29] Adding MA, Cs or Rb have been shown to prevent this degradation.[30–32]

One possible contribution to the greater long term stability of mixed cation perovskites comes from the suppression of iodide diffusion.[5,32–35] This has been observed as an increase in activation energy for anion motion upon cation-mixing at the A-site of methylammonium lead iodide.[17,36]

Department of Chemistry, University of Bath, Bath, BA2 7AY, UK.
E-mail: s.r.pering@lboro.ac.uk

† Electronic supplementary information (ESI) available: Experimental methods and Supplementary Figures. See DOI: https://doi.org/10.1039/d2ma00619g

‡ Samuel R. Pering current address: Department of Materials, Loughborough University, LE11 3TU, UK.

© 2022 The Author(s). Published by the Royal Society of Chemistry

Open Access Article. Published on 23 August 2022. Downloaded on 5/3/2026 9:02:49 AM.
This article is licensed under a Creative Commons Attribution 3.0 Unported Licence.

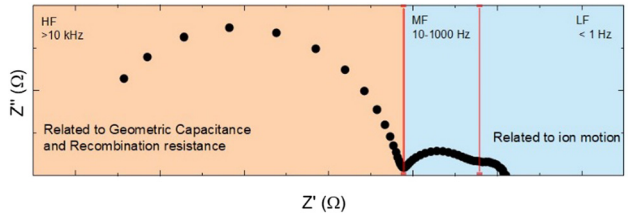

Fig. 1 Idealised MAPI impedance spectrum (Nyquist plot), showing high (HF), mid (MF) and low (LF) frequency regions, and areas on spectrum related to different processes (orange and blue).

An increase in activation energy for ion motion has also been observed when mixing occurs at either the B or X-site.[37–40] Previous EIS studies on FAPI have shown that, as in MAPI, the high frequency response does not change greatly with the addition of more components; it is the lower frequency responses that are altered.[41,42] Few temperature dependent measurements have been performed on FAPI based perovskites to attempt to extract activation energies. In this report the effects of substitution at both the A and X site of FAPI are investigated, to determine if there are any beneficial synergistic effects of the triple-cation $Cs_{0.05}(FA_{0.83}MA_{0.17}Pb(I_{0.83}Br_{0.17})_3)$ perovskite with regards to suppression of ion migration.

Results and discussion

PSC made with MAPI have been extensively measured by EIS, and the high frequency (HF) electronic response is reasonably well understood. The HF response is typically dominated by the geometric capacitance and the recombination resistance.[15,16,43] There is less consensus on the origin of the low frequency impedance.[16,41,42,44–51] In impedance measurements we measure a current that is created by applying a sinusoidally modulated voltage to the system. We measure at open circuit (V_{OC}) under illumination and apply ± 10 mV modulation around the cell's open circuit value. By applying a voltage slightly less than or more than the V_{OC}, we measure a current that is strongly dependent on the rate of electron–hole recombination within the device. At high frequencies, typically above 10^4 Hz, the field is varying too quicky for ions to respond and we measure the electronic response from our system which, as already mentioned, is dominated by the geometric capacitance (the capacitance when the perovskite is depleted) and the recombination resistance. This characteristic frequency of the HF response does not vary greatly with temperature.[16,17]

The two lower frequency responses (labelled MF and LF in Fig. 1) occur when the applied voltage is varying on a timescale in which the ions can move to redistribute themselves with the field. We have previously argued that ion motion can act to modify the recombination resistance (and hence the current), and that the low frequency impedance response is due to a frequency dependent recombination resistance.[16] Jacobs *et al.* also tie the low frequency impedance response to ion modulated recombination currents.[52] Ebadi *et al.* take a related approach where it is injection, rather than recombination, which is assumed to be modified by the ionic distribution.[47] Similarly, in the model created by Moia *et al.* it is shown that the accumulation or depletion of ionic charge at the interfaces of the device modulates barriers to injection and recombination, allowing the authors to account for the impedance response of perovskite devices.[50] Finally modelling by Riquelme *et al.* attributes the low frequency response to a 'recombination resistance modulated by ion transport from the bulk to/from the Debye layers'.[49] It is possible to explain all the exotic features observed in the impedance spectrum, including negative capacitances, induction loops and giant capacitance by understanding how slow moving ions act to modify the (photo)current. What is clear, is that the time constants for the low frequency features, MF and LF, are linked to the ion diffusion coefficient,[49] and that information about ion motion can be extracted from temperature dependent impedance measurements. In MAPI both the LF and MF responses have been linked to iodide motion, with an activation energy for bothprocesses of 0.35 eV to 0.5 eV. The main difference between the MF and LF processes is the 'attempt frequency'. The MF process has a measured attempt frequency that is usually 1–2 orders of magnitude higher than that of the low frequency process (typically MF is 10^{10}–10^{11} s^{-1} and the LF is $\sim$ 10^9–10^{10} s^{-1}). In the case of the LF signal, the measured activation energy is highly dependent on the composition of the perovskite.,[16,17,36,37,39] and both cation and anion substitution strongly modify E_A by introducing local distortions.[17] This could suggest that the LF semi-circle is due to the modulation of ions (most likely iodide) inside the perovskite grains. Although cation migration possesses a similar activation energy, the timescale of this process is outside the experimental window, therefore iodide migration is the most likely measured process.[53] The MF process is similarly temperature dependent, but the only experimental way we have found to modify the MF activation energy is through Rb^+ or Cs^+ substitution into MAPI.[17] The same trend is seen in the results presented in Table 1. When Cs is added to FAPI, the E_A of the MF

Table 1 Values calculated by impedance for FAPI based perovskites – graphs in Fig. S5–S9 (ESI). MF and LF denote mid-frequency and low-frequency respectively

Cation	R_{ct} (Ω) (at 25 °C)	C_{geo} (nF) (at 25 °C)	τMF (ms) (at 25 °C)	τLF (ms) (at 25 °C)	E_a (eV) (MF)	E_a (eV) (LF)
$FAPbI_3$	18.75	22.7	0.32	Not visible	0.37 ± 0.02	Not visible
$FA_{0.83}MA_{0.17}PbI_3$	38	9.4	0.83	43	0.37 ± 0.03	0.53 ± 0.01
$Cs_{0.05}(FA_{0.83}MA_{0.17})_{0.95}PbI_3$	17.7	18.0	0.22	25	0.53 ± 0.01	0.21 ± 0.02
$FA_{0.83}MA_{0.17}Pb(I_{0.83}Br_{0.17})_3$	241	10.5	Not visible	23	Not visible	0.38 ± 0.03
$Cs_{0.05}(FA_{0.83}MA_{0.17})_{0.95}Pb(I_{0.83}Br_{0.17})_3$	282	14.0	0.57	43	0.45 ± 0.02	0.81 ± 0.07

Open Access Article. Published on 23 August 2022. Downloaded on 5/3/2026 9:02:49 AM.
This article is licensed under a Creative Commons Attribution 3.0 Unported Licence.

process increases from 0.37 eV to 0.53 eV. There is some evidence that small A site cations can preferentially sit on the surface of the perovskite crystallites, passivating defects and making it harder for ions to migrate along the grain boundaries.[54,55] We therefore suspect that the MF response is due to ion (again most likely iodide) diffusion along grain boundaries and interfaces with the contact layers. At very low frequencies, the impedance spectrum extends beyond the initial quadrant,[56] and care has to be taken when interpreting these results as the low frequency data often fail a Kramers–Kronig transformation test; this checks the relationship between the real and imaginary impedance, suggesting whether or not a valid impedance response is being measured.[57]

In this study we look at the effect of cation and anion mixing on the impedance response of FAPI based perovskite solar cells. We started by measuring FAPI cells, taking great care to make and measure the cells rapidly to ensure that they remained predominately in the cubic perovskite phase. The components of $Cs_{0.05}(FA_{0.83}MA_{0.17})_{0.95}Pb(I_{0.83}Br_{0.17})_3$ were then added individually to form 4 different combinations, to probe the effect each additive has on ion diffusion within the cell. We prepared and measured inverted NiO_X/FAPI/PCBM cells as they show enhanced stability during impedance measurements. $FAPb(I_{0.83}Br_{0.17})_3$ was not included for comparison, as the band gap is shifted significantly and resulting solar cells have lower efficiencies compared to the other samples.

Like MAPI, FAPI is a 3D perovskite, however in this case it is almost cubic at room temperature.[26] X-Ray diffractograms are shown in Fig. 2. Upon substitution at the A or X-site the structure is distorted. The distortion effect occurs to a much greater extent with Br^- substitution, as shown in Fig. 2(a), where the 002 peak is shifted significantly to higher 2θ values in the two bromide containing materials; closer to the values shown by the 220 peak in MAPI ($\sim 29.5^\circ$ 2θ).[17]

The UV/Vis spectroscopy showed a slight blue shift caused by X-site substitution (Fig. S1, ESI†). The performance of cells containing varying amounts of A and X-site substitution up to the ratio for the triple-cation perovskite is shown in Table S1 and Fig. S2 (ESI†). A representative JV curve for $Cs_{0.05}(FA_{0.83}MA_{0.17})_{0.95}Pb(I_{0.83}Br_{0.17})_3$ is shown in Fig. S2e (ESI†)

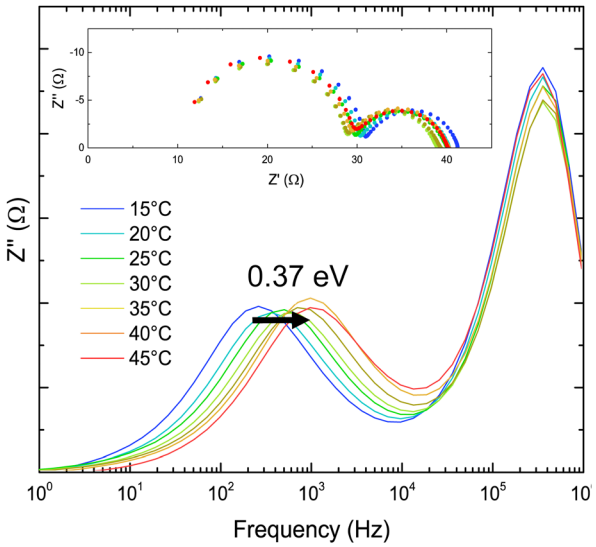

Fig. 3 The Impedance response of FAPbI3 with temperature, Cole plots with activation energy overlayed, and inset Nyquist plots.

and shows low hysteresis. In this study we analysed cells of similar efficiency and particularly open-circuit voltage, to avoid differences that occur with a change in performance. This means that we have not selected the most efficient cells, rather those that are most similar in terms of V_{OC} and J_{sc}, allowing for a more reliable analysis of the AC response. EIS was measured at 7 temperatures between 45 °C and 15 °C, the range in which the low frequency responses attributed to the effects of iodide diffusion were most visible in previous studies.[16,17]

The impedance spectra for FAPI, used as a baseline in this study, are shown in Fig. 3. All cells were measured within 1 day of initial fabrication, as the stability of FAPI cells goes below 80% original efficiency after 3 days (Fig. S3, ESI†). There are 5 components to the most efficient perovskite, and cations and anions were added to FAPI individually to build a picture of the changes when forming $Cs_{0.05}(FA_{0.83}MA_{0.17})_{0.95}Pb(I_{0.83}Br_{0.17})_3$. Cell characterisation data are shown in Table 1 and Fig. S5–S9 (ESI†).

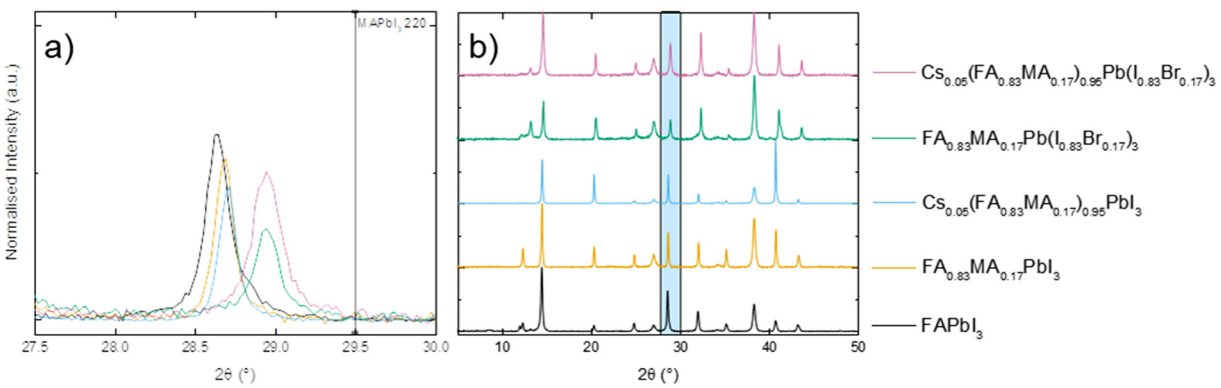

Fig. 2 XRD analysis of perovskites (a) zoomed in image showing peaks in relation to MAPI 220 peak, and (b) full PXRD spectrum with zoomed in region highlighted.

© 2022 The Author(s). Published by the Royal Society of Chemistry

Open Access Article. Published on 23 August 2022. Downloaded on 5/3/2026 9:02:49 AM.
This article is licensed under a Creative Commons Attribution 3.0 Unported Licence.

For FAPI, two semi-circles were observed in the Nyquist plots between 1 MHz and 10 Hz. The high frequency semicircle, between 1 MHz and 10 kHz, is consistent with the recombination resistance and geometric capacitance, and does not vary with temperature.[15,16] Comparison with our previous impedance studies suggests that the second semi-circle, between 10 kHz and 10 Hz, is the MF response.[16,17,38]

Effect of cation and anion substitution on the mid-frequency response of PSC

The mid-frequency feature for FAPI cells is temperature dependent and has an activation energy of 0.37 eV. This activation barrier is very similar to those previously extracted for the mid-frequency response of MAPI.[16,17,38] Surface analysis of FAPI (Fig. S4, ESI†) undertaken by AFM reveal a surface with small, densely packed crystallites of similar morphology to our MAPI films. If the MF response is due to ion motion at grain boundaries, then the similar morphology of both systems would corroborate this theory.

In the mid-frequency portion of the spectrum, the addition of 17 mol% MA^+ does not change the activation energy. In contrast, addition of 5 mol% Cs^+ causes the activation energy to increase to 0.53 eV. As mentioned above, this is consistent with our previous results for MAPI where adding 5% Cs^+ or 5% Rb^+ increased the activation energy of the MF process. Again this suggests that at MF we could be measuring the effects of ions migrating at grain boundaries and that Cs^+ is acting to passivate the crystallite surfaces.[58,59] The effect of bromide substitution on the mid-frequency process, measured for cells containing $FA_{0.83}MA_{0.17}Pb(I_{0.83}Br_{0.17})_3$, is unclear as in this case it is only observed as a shoulder to the HF semicircle, and provides insufficient data to create an Arrhenius plot.

Effect of cation and anion substitution on the low frequency response of PSC

It is interesting that the low frequency response observed below 1 Hz in MAPI cells, is absent in FAPI Cells. As mentioned above, the LF response in MAPI cells is strongly dependent on the composition of the perovskite. Substituting in ions that vary in size with respect to those in the parent material causes local distortions to the lattice that can influence the activation energy for ion migration. One major difference between MAPI and FAPI is the octahedral-corrected Goldschmidt tolerance factor, which is 0.95 for MAPI and 1.03 for FAPI.[60] The FAPI perovskite lattice is therefore more strained, which can modify the activation energy for iodide motion.[61] Computational studies of FAPI suggest activation energies of 0.45 eV to 0.50e V for iodide vacancies,[22,62] similar to the values in MAPI. The high lattice strain can also reduce the energy of defect formation.[63] Riquelme *et al.* used drift diffusion modelling to investigate the influence of iodide diffusion coefficient and iodide vacancy density on the impedance response of perovskite solar cells. They show that increasing the diffusion coefficient (which would relate to a lower activation energy) moves the LF response to higher frequencies. Reducing the number of iodide vacancies caused the LF response to first decrease in magnitude, before moving below the axis to show a response in the fourth quadrant. The absence of the LF response in FAPI is most likely explained by a decrease in activation energy for ion migration inside the FAPI crystallites caused by high lattice strain. This would cause the LF response to move to higher frequencies and to be hidden by the high frequency and MF responses. A change in the defect density could also change the magnitude of the LF impedance making it harder to detect. In a previous study we found that the LF response is also absent in cells containing $MAPbBr_3$, which has a tolerance factor of 0.99. It is likely a similar explanation can be used for both $MAPbBr_3$ and FAPI cells.

In the bromide-free perovskites, the addition of the cations (both of which are smaller than FA) results in the re-appearance of the low-frequency semi-circle. The LF activation energy for $FA_{0.83}MA_{0.17}PbI_3$ is 0.53 eV. Adding 5 mol% Cs^+ to $FA_{0.83}MA_{0.17}PbI_3$ reduces the activation energy from 0.53 eV (Fig. S6, ESI†) to 0.21 eV (Fig. S7, ESI†). These results contrast those observed in the tetragonal structure of MAPI where distortion of the lattice caused by cation substitution increased the activation energy. In FAPI it has been shown that adding MA^+ and Cs^+ can reduce the strain in the material,[64] it is not currently clear why Cs^+ addition should increase the activation energy for ion motion in MAPI but reduce it in FAPI.

Mixing the halide composition to give $FA_{0.83}MA_{0.17}Pb(I_{0.83}Br_{0.17})_3$ completely changes the impedance spectrum. There is a tenfold increase in the recombination resistance, R_{rec} after bromide addition. This increase in R_{rec} with no change in C_{geo} means that the time constant for the HF process is significantly shifted with respect to the iodide perovskites. Previous studies have shown that bromide diffusion is not visible on the timescale of the impedance experiment, so the low-frequency element is due to iodide ion diffusion.[38] The low frequency feature is visible (Fig. S8, ESI†), and from the Arrhenius plot an activation energy of 0.38 eV is calculated.

Impedance spectra of triple-cation PSC

For the state-of-the-art triple-cation perovskite, a Nyquist plot for $Cs_{0.05}(FA_{0.83}MA_{0.17})_{0.95}Pb(I_{0.83}Br_{0.17})_3$ is shown in Fig. 4. Substitution at both the A and X-sites has resulted in a spectrum that takes features from both, *i.e.* the recombination resistance is still ten-fold larger than for FAPI (caused by Br^- substitution), but there are once again three semi-circles visible in the Nyquist plot.

The interesting combination of substitution at two sites extends into the trends shown when the impedance is measured over a range of temperatures (Fig. 4). The activation energy for the low frequency process is 0.81 eV – even within the increased margin of error of $\pm$ 0.07 compared to the other samples, this is a dramatic increase on the 0.21 eV shown by $Cs_{0.05}(FA_{0.83}MA_{0.17})_{0.95}PbI_3$ and the largest value we have ever measured for either a MAPI or FAPI based perovskite solar cell, with similar photovoltaic parameters. The mid-frequency process has an E_A of 0.45 eV. From the data available in Table 1 it is clear that once again Cs^+ is having an effect on the process occurring in the mid-frequency range.

Open Access Article. Published on 23 August 2022. Downloaded on 5/3/2026 9:02:49 AM.
This article is licensed under a Creative Commons Attribution 3.0 Unported Licence.

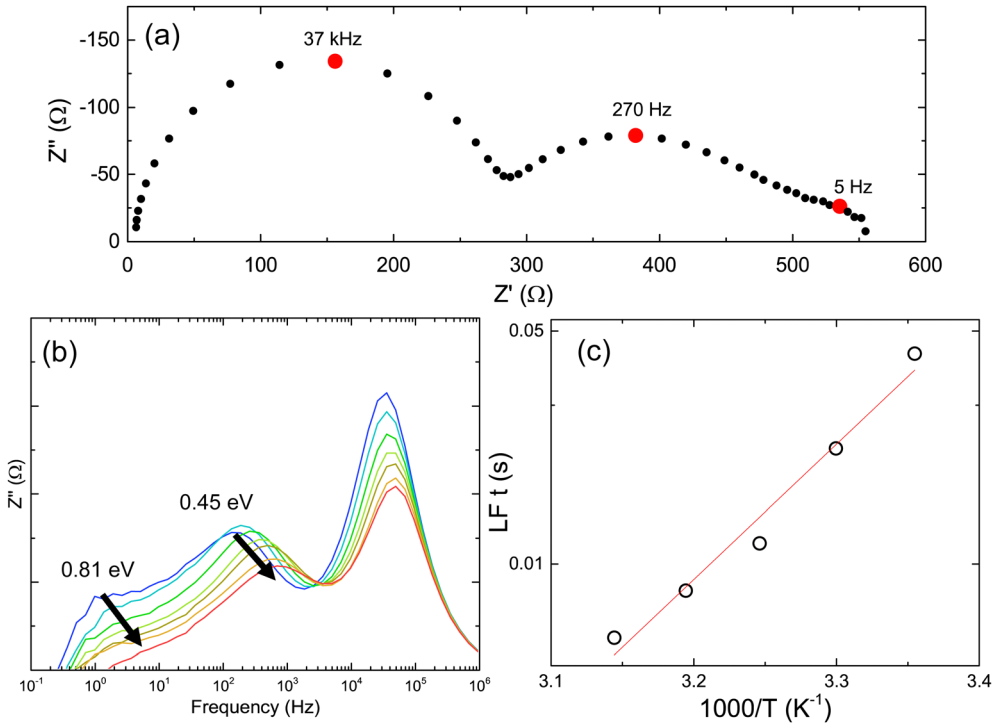

Fig. 4 Impedance of $Cs_{0.05}(FA_{0.83}MA_{0.17})_{0.95}Pb(I_{0.83}Br_{0.17})_3$: (a) Nyquist plot at 25 °C, (b) Cole plots with temperature including activation energy for mid- and low-frequency process, and (c) Arrhenius plot for the Low Frequency feature.

Fig. 5 shows both the LF activation energy, and the Goldschmidt tolerance factor plotted against the shift in 2θ of the 002 peak with respect to FAPI in the substituted perovskites. The tolerance factor for the mixed perovskites was estimated by simply taking ratios of the ionic radii for the different ions in the mixed phase. Interestingly both E_A and t show a similar dependence on 2θ, there is also a clear separation between the iodide and the mixed halide perovskites with respect to 2θ. There is no clear trend in E_A with tolerance factor. It is likely that ion migration is controlled by complex local interactions in the lattice and that the calculated tolerance factors are a gross oversimplification of the picture.

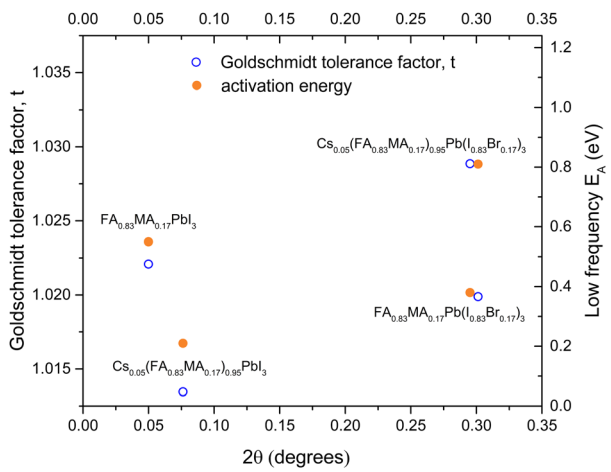

Fig. 5 Graph of activation energy and Goldschmidt Tolerance factor against shift in 2θ from the FAPI 002 peak.

Conclusions

In this report we have measured iodide diffusion by electrochemical impedance spectroscopy in substituted perovskite solar cellsbased on the parent structure of formamidinium lead iodide. FAPI cells show a different impedance response to MAPI ones, with only two semi-circles visible in the Nyquist plot. Despite this the mid-frequency response of cells containing MAPI or FAPI display similar time constants and activation energies, suggesting a common, cation-independent process is happening on this timescale.

Structural substitutions into FAPI significantly alter the measured LF activation energies for iodide diffusion in the materials. Increasing substitution of smaller cations, cesium and methylammonium, reduces the activation energy. Substituting both the A-site cation and the X-site halide anion leads to a tenfold increase in the R_{ct} value. The triple-cation perovskite, $Cs_{0.05}(FA_{0.83}MA_{0.17})_{0.95}Pb(I_{0.83}Br_{0.17})_3$, exhibits a higher barrier to ion diffusion (0.81 eV) than previously measured for MAPI or FAPI, this result provides additional understanding of to the high performance of triple cation perovskite solar cells.

Author contributions

S. R. P. involved in conceptualisation, investigation, methodology, analysis and writing – original draft; P. J. C. involved in

© 2022 The Author(s). Published by the Royal Society of Chemistry

conceptualisation, funding acquisition, project administration, supervision and writing – review and editing.

Conflicts of interest

There are no conflicts to declare.

Acknowledgements

S. R. P thanks the University of Bath for Studentship (Grant number 1651392). S. R. P thanks Loughborough University for Research Funding.

Notes and references

1 A. Kojima, K. Teshima, Y. Shirai and T. Miyasaka, *J. Am. Chem. Soc.*, 2009, **131**, 6050–6051.
2 M. Saliba, T. Matsui, J.-Y. Seo, K. Domanski, J.-P. Correa-Baena, N. Mohammad, K. S. M. Zakeeruddin, W. Tress, A. Abate, A. Hagfeldt and M. Grätzel, *Energy Environ. Sci.*, 2016, **9**, 1989–1997.
3 M. M. Lee, J. Teuscher, T. Miyasaka, T. N. Murakami and H. J. Snaith, *Science*, 2012, **338**, 643–647.
4 H. Tsai, W. Nie, J. C. Blancon, C. C. Stoumpos, R. Asadpour, B. Harutyunyan, A. J. Neukirch, R. Verduzco, J. J. Crochet, S. Tretiak, L. Pedesseau, J. Even, M. A. Alam, G. Gupta, J. Lou, P. M. Ajayan, M. J. Bedzyk, M. G. Kanatzidis and A. D. Mohite, *Nature*, 2016, **536**, 312–317.
5 G. Grancini, C. Roldán-Carmona, I. Zimmermann, E. Mosconi, X. Lee, D. Martineau, S. Narbey, F. Ostwald, F. De Angelis, M. Graetzel and M. K. Nazeeruddin, *Nat. Commun.*, 2017, **8**, 15684.
6 J. Yen-Sook, H. Kyeongil, H. Youn-Jung, K. Jueng-Eun, V. Doojin and K. Dong-Yu, *Adv. Opt. Mater.*, 2018, **0**, 1701182.
7 K. Hwang, Y. S. Jung, Y. J. Heo, F. H. Scholes, S. E. Watkins, J. Subbiah, D. J. Jones, D. Y. Kim and D. Vak, *Adv. Mater.*, 2015, **27**, 1241–1247.
8 G. Divitini, S. Cacovich, F. Matteocci, L. Cinà, A. Di Carlo and C. Ducati, *Nat. Energy*, 2016, **1**, 15012.
9 G. Abdelmageed, L. Jewell, K. Hellier, L. Seymour, B. Luo, F. Bridges, J. Z. Zhang and S. Carter, *Appl. Phys. Lett.*, 2016, **109**, 233905.
10 S. Zhaoning, A. Antonio, S. Watthage, G. Liyanage, A. Phillips, U. Steiner, M. Graetzel and M. Heben, *Adv. Energy Mater.*, 2016, **6**, 1600846.
11 N. Aristidou, C. Eames, I. Sanchez-Molina, X. Bu, J. Kosco, M. Saiful Islam and S. A. Haque, *Nat. Commun.*, 2017, **8**, 15218.
12 G. Richardson, S. E. J. O'Kane, R. G. Niemann, T. A. Peltola, J. M. Foster, P. J. Cameron and A. B. Walker, *Energy Environ. Sci.*, 2016, **9**, 1476–1485.
13 B. Chen, M. Yang, X. Zheng, C. Wu, W. Li, Y. Yan, J. Bisquert, G. Garcia-Belmonte, K. Zhu and S. Priya, *J. Phys. Chem. Lett.*, 2015, **6**, 4693–4700.
14 Y. Zhao, W. Zhou, Z. Han, D. Yu and Q. Zhao, *Phys. Chem. Chem. Phys.*, 2021, **23**, 94–106.
15 A. Pockett, G. E. Eperon, T. Peltola, H. J. Snaith, A. Walker, L. M. Peter and P. J. Cameron, *J. Phys. Chem. C*, 2015, **119**, 3456–3465.
16 A. Pockett, G. E. Eperon, N. Sakai, H. J. Snaith, L. M. Peter and P. J. Cameron, *Phys. Chem. Chem. Phys.*, 2017, **19**, 5959–5970.
17 D. W. Ferdani, S. R. Pering, D. Ghosh, P. Kubiak, A. B. Walker, S. E. Lewis, A. L. Johnson, P. J. Baker, M. S. Islam and P. J. Cameron, *Energy Environ. Sci.*, 2019, **12**, 2264–2272.
18 B. Li, C. Kan, P. Hang, Y. Fang, L. Zuo, L. Song, Y. Zhang, D. Yang and X. Yu, *Phys. Status Solidi RRL*, 2021, **15**, 2100225.
19 C. Eames, J. M. Frost, P. R. F. Barnes, B. C. O'Regan, A. Walsh and M. S. Islam, *Nat. Commun.*, 2015, **6**, 7497.
20 A. Baumann, S. Väth, P. Rieder, M. C. Heiber, K. Tvingstedt and V. Dyakonov, *J. Phys. Chem. Lett.*, 2015, **6**, 2350–2354.
21 O. Almora, I. Zarazua, E. Mas-Marza, I. Mora-Sero, J. Bisquert and G. Garcia-Belmonte, *J. Phys. Chem. Lett.*, 2015, **6**, 1645–1652.
22 J. Haruyama, K. Sodeyama, L. Han and Y. Tateyama, *J. Am. Chem. Soc.*, 2015, **137**, 10048–10051.
23 S. Meloni, T. Moehl, W. Tress, M. Franckevičius, M. Saliba, Y. H. Lee, P. Gao, M. K. Nazeeruddin, S. M. Zakeeruddin, U. Rothlisberger and M. Graetzel, *Nat. Commun.*, 2016, **7**, 10334.
24 C. Li, S. Tscheuschner, F. Paulus, P. E. Hopkinson, J. Kießling, A. Köhler, Y. Vaynzof and S. Huettner, *Adv. Mater.*, 2016, **28**, 2446–2454.
25 M. T. Weller, O. J. Weber, P. F. Henry, A. M. Di Pumpo and T. C. Hansen, *Chem. Commun.*, 2015, **51**, 4180–4183.
26 M. T. Weller, O. J. Weber, J. M. Frost and A. Walsh, *J. Phys. Chem. Lett.*, 2015, **6**, 3209–3212.
27 S. Pang, H. Hu, J. Zhang, S. Lv, Y. Yu, F. Wei, T. Qin, H. Xu, Z. Liu and G. Cui, *Chem. Mater.*, 2014, **26**, 1485–1491.
28 W. Shockley and H. J. Queisser, *J. Appl. Phys.*, 1961, **32**, 510–519.
29 C. C. Stoumpos, C. D. Malliakas and M. G. Kanatzidis, *Inorg. Chem.*, 2013, **52**, 9019–9038.
30 C. Yi, J. Luo, S. Meloni, A. Boziki, N. Ashari-Astani, C. Gratzel, S. M. Zakeeruddin, U. Rothlisberger and M. Gratzel, *Energy Environ. Sci.*, 2016, **9**, 656–662.
31 M. Salado, S. Kazim and S. Ahmad, *Chem. Pap.*, 2018, **72**, 1645–1650.
32 D. Ghosh, P. Walsh Atkins, M. S. Islam, A. B. Walker and C. Eames, *ACS Energy Lett.*, 2017, **2**, 2424–2429.
33 M. Saliba, M. Saliba, T. Matsui, K. Domanski, J.-Y. Seo and A. Ummadisingu, *Science*, 2016, **354**, 206–209.
34 S. Reichert, J. Flemming, Q. An, Y. Vaynzof, J.-F. Pietschmann and C. Deibel, *Phys. Rev. Appl.*, 2020, **13**, 34018.
35 D. Lan, *Prog. Photovolt. Res. Appl.*, 2020, **28**, 533–537.
36 S. Tan, I. Yavuz, N. De Marco, T. Huang, S.-J. Lee, C. S. Choi, M. Wang, S. Nuryyeva, R. Wang, Y. Zhao, H.-C. Wang,

Open Access Article. Published on 23 August 2022. Downloaded on 5/3/2026 9:02:49 AM. This article is licensed under a Creative Commons Attribution 3.0 Unported Licence.

Open Access Article. Published on 23 August 2022. Downloaded on 5/3/2026 9:02:49 AM. This article is licensed under a Creative Commons Attribution 3.0 Unported Licence.

T.-H. Han, B. Dunn, Y. Huang, J.-W. Lee and Y. Yang, *Adv. Mater.*, 2020, **32**, 1906995.
37 N. Rybin, D. Ghosh, J. Tisdale, S. Shrestha, M. Yoho, D. Vo, J. Even, C. Katan, W. Nie, A. J. Neukirch and S. Tretiak, *Chem. Mater.*, 2020, **32**, 1854–1863.
38 R. García-Rodríguez, D. Ferdani, S. Pering, P. J. Baker and P. J. Cameron, *J. Mater. Chem. A*, 2019, **7**, 22604–22614.
39 M. H. Futscher, M. K. Gangishetty, D. N. Congreve and B. Ehrler, *ACS Appl. Electron. Mater.*, 2020, **2**, 1522–1528.
40 P. Srivastava, R. Kumar and M. Bag, *J. Phys. Chem. C*, 2021, **125**, 211–222.
41 O. Almora, K. T. Cho, S. Aghazada, I. Zimmermann, G. J. Matt, C. J. Brabec, M. K. Nazeeruddin and G. Garcia-Belmonte, *Nano Energy*, 2018, **48**, 63–72.
42 P. Wang, M. Ulfa and T. Pauporte, *J. Phys. Chem. C*, 2018, **122**, 1973–1981.
43 A. Bou, A. Pockett, D. Raptis, T. Watson, M. J. Carnie and J. Bisquert, *J. Phys. Chem. Lett.*, 2020, **11**, 8654–8659.
44 D. Zheng, T. Zhu and T. Pauporté, *ACS Appl. Energy Mater.*, 2020, **3**, 10349–10361.
45 L. Contreras-Bernal, S. Ramos-Terrón, A. Riquelme, P. P. Boix, J. Idígoras, I. Mora-Seró and J. A. Anta, *J. Mater. Chem. A*, 2019, **7**, 12191–12200.
46 R. Jacobs, G. Luo and D. Morgan, *Adv. Funct. Mater.*, 2019, **29**, 1804354.
47 F. Ebadi, N. Taghavinia, R. Mohammadpour, A. Hagfeldt and W. Tress, *Nat. Commun.*, 2019, **10**, 1574.
48 M. A. Afroz, C. A. Aranda, N. K. Tailor, Yukta, P. Yadav, M. M. Tavakoli, M. Saliba and S. Satapathi, *ACS Energy Lett.*, 2021, **6**, 3275–3286.
49 A. Riquelme, L. J. Bennett, N. E. Courtier, M. J. Wolf, L. Contreras-Bernal, A. B. Walker, G. Richardson and J. A. Anta, *Nanoscale*, 2020, **12**, 17385–17398.
50 D. Moia, I. Gelmetti, P. Calado, W. Fisher, M. Stringer, O. Game, Y. Hu, P. Docampo, D. Lidzey, E. Palomares, J. Nelson and P. R. F. Barnes, *Energy Environ. Sci.*, 2019, **12**, 1296–1308.
51 E. von Hauff and D. Klotz, *J. Mater. Chem. C*, 2022, **10**, 742–761.
52 D. A. Jacobs, H. Shen, F. Pfeffer, J. Peng, T. P. White, F. J. Beck and K. R. Catchpole, *J. Appl. Phys.*, 2018, **124**, 225702.
53 K. Domanski, B. Roose, T. Matsui, M. Saliba, S.-H. Turren-Cruz, J.-P. Correa-Baena, C. R. Carmona, G. Richardson, J. M. Foster, F. De Angelis, J. M. Ball, A. Petrozza, N. Mine, M. K. Nazeeruddin, W. Tress, M. Grätzel, U. Steiner, A. Hagfeldt and A. Abate, *Energy Environ. Sci.*, 2017, **10**, 604–613.
54 C. Xu, X. Chen, S. Ma, M. Shi, S. Zhang, Z. Xiong, W. Fan, H. Si, H. Wu, Z. Zhang, Q. Liao, W. Yin, Z. Kang and Y. Zhang, *Adv. Mater.*, 2022, 2109998.
55 F. Han, J. Luo, B. Zhao, Z. Wan, R. Wang and C. Jia, *Electrochim. Acta*, 2017, **236**, 122–130.
56 A. Pockett, M. Spence, S. K. Thomas, D. Raptis, T. Watson and M. J. Carnie, *Sol. RRL*, 2021, **5**, 2100159.
57 M. Schönleber, D. Klotz and E. Ivers-Tiffée, *Electrochim. Acta*, 2014, **131**, 20–27.
58 Y. Zhao, Y. Zhao, W. Zhou, Q. Li, R. Fu, D. Yu and Q. Zhao, *ACS Appl. Mater. Interfaces*, 2018, **10**, 33205–33213.
59 G. Tong, H. Li, G. Li, T. Zhang, C. Li, L. Yu, J. Xu, Y. Jiang, Y. Shi and K. Chen, *Nano Energy*, 2018, **48**, 536–542.
60 W. Travis, E. N. K. Glover, H. Bronstein, D. O. Scanlon and R. G. Palgrave, *Chem. Sci.*, 2016, **7**, 4548–4556.
61 L. Jin-Wook, T. Shaun, S. S. Il, Y. Yang and P. Nam-Gyu, *Science*, 2022, **375**, eabj1186.
62 J. M. Cave, N. E. Courtier, I. A. Blakborn, T. W. Jones, D. Ghosh, K. F. Anderson, L. Lin, A. A. Dijkhoff, G. J. Wilson, K. Feron, M. Saiful Islam, J. M. Foster, G. Richardson and A. B. Walker, *J. Appl. Phys.*, 2020, **128**, 184501.
63 T. W. Jones, A. Osherov, M. Alsari, M. Sponseller, B. C. Duck, Y.-K. Jung, C. Settens, F. Niroui, R. Brenes, C. V. Stan, Y. Li, M. Abdi-Jalebi, N. Tamura, J. E. Macdonald, M. Burghammer, R. H. Friend, V. Bulović, A. Walsh, G. J. Wilson, S. Lilliu and S. D. Stranks, *Energy Environ. Sci.*, 2019, **12**, 596–606.
64 K. Gwisu, M. Hanul, L. K. Su, L. Do Yoon, Y. S. Me and S. S. Il, *Science*, 2020, **370**, 108–112.

© 2022 The Author(s). Published by the Royal Society of Chemistry